Nanoscale Res Lett (2010) 5:138–142
DOI 10.1007/s11671-009-9455-y

NANO EXPRESS

Obvious Temperature Difference Along a Pb Cluster-Decorated Carbon Nanowire

Fengqi Song · Longbing He · Min Han · Jianguo Wan · Guanghou Wang

Received: 22 July 2009 / Accepted: 25 September 2009 / Published online: 10 October 2009

Abstract Pb nanoclusters were deposited onto a suspended carbon nanowire (CNW), where in situ temperature variable observation was carried out by a transmission electron microscope. The heating temperature was up to 450 °C. Both the melting and evaporation of the Pb nanoparticles on the CNW were retarded when compared to the particles on the support frame. The obvious temperature difference of up to 10 K along the CNW of less than 1 μm was demonstrated. It was attributed to the irradiating dissipation-dependent on the surface area of the decorating Pb particle by calculation.

Keywords Temperature difference · Retarded melting · Thermal transportation · Pb · Cluster · Carbon nanowire

Introduction

Much attention has been paid to the sub-micrometer scale thermal transportation along a nanowire mainly due to the scale-dependent carrier behavior upon nanoconfinement and their potential application in the thermoelectric devices and thermoresistive coating materials [1–7]. One of the key problems is the temperature difference (TD) between two ends of the nanowire [8–10]. However, the TD on the sub-nanometer scale (or even on a few micrometers) keeps rather small. It will diminish to a very small value in less than 1 second, even if a highly thermal insulating material is employed. It is because the power of thermal conduction from the end of the high temperature to that of the low temperature is much higher than the thermal dissipation if there is a considerable TD. As the result, only the TD of 0.2 K was observed along a single wall carbon nanotube of 2 μm [10]. Even, the well-known thermoelectric candidate of Bi nanowire produced a small TD of 4 K along the length of 15 μm [2, 11, 12]. The measurement of these small values of the TDs requires some deliberately designed MEMS devices and complex procedures to make precise calibration of local temperatures [7, 13, 14]. In this work, carbon nanowires (CNWs) were suspended on a holey support film, and then Pb nanoclusters were deposited on the sample in situ temperature variable transmission electron microscopic (TEM) observation demonstrated the obvious TD of up to 10 K along the CNW of less than 1 μm.

On the other hand, the present TD permits the intuitivistic visualization of the nanoscale thermal inhomogeneity. Nanostructures of the low melting point nanoparticles (Pb, Ga or even Zn) have long been featured for their thermal effects, such as the freezing behavior [15, 16], phase oscillation between liquid and solid [17] and the liquid nanojet from the core expansion ([18], see the supplementary materials also). In the normal heating carried out through broad contacts, the earlier mentioned thermal effects occurred abruptly ([16, 18], see the supplementary materials also). The detailed explanation of the experiment desires decomposed visualizations. However, it is only possible

Electronic supplementary material The online version of this article (doi:10.1007/s11671-009-9455-y) contains supplementary material, which is available to authorized users.

F. Song (✉) · J. Wan · G. Wang
National Laboratory of Solid State Microstructures and Department of Physics, Nanjing University, 210093 Nanjing, China
e-mail: songfengqi@nju.edu.cn

L. He · M. Han
National Laboratory of Solid State Microstructures and Department of Materials Science and Engineering, Nanjing University, 210093 Nanjing, China

during controlled heating. In our work, heat is expected to input to the particle on CNW (POC) through the CNW, which limits the thermal input by changing the 2-dimensional (D) contact of the particle on the support (POS) to 1-D transportation. The retardations of the POC's melting and evaporation were then decomposedly visualized.

Experimental Details

The CNW was prepared in a radiofrequency plasma sputtering chamber, where a small nozzle to the high-vacuum chamber led the CNW onto the TEM copper meshes with holey support films. Only enough long CNWs were suspended on the microsized pores. TEM, High-resolution TEM and electron energy loss spectra (EELS) proved their amorphous structures (see the supplementary materials also, [19]). The beam of Pb nanoclusters was generated by a gas aggregation cluster source and deposited onto the copper mesh [18]. A TEM of Jeol 200CX was employed for the in situ observation, and the process was recorded by a digital video system.

Figure 1a shows a TEM image from the region of interest, where we can see the Pb particles are distributed on the support film and on the CNW simultaneously. The CNWs with the diameters of 10–20 nm are suspended on the pore, on which a Pb nanoparticle with the size of about 130 nm sits. The system was heated through a heating holder and the thermocouple sensor recorded the heating temperatures in a temperature-fixing mode. The thermal conduction between the heating source and the copper mesh was enhanced by two pressed nickel grids. The holey support film was attached to the copper mesh, and all the region in the support film was within a few micrometers from the copper grid. It guarantees the efficient heating of the support film. Therefore, we regard the temperature from the thermocouple meter as the temperature on the amorphous support. POS was heated more effectively than POC due to the 2-D transporting routes (see Fig. 1b). We track the melting of the Pb particles to show the thermal effect.

Result and Discussion

Here two phenomena are identified as the signatures of the particles' melting. One of them is the abrupt change of the contrast, which can be seen in Fig. 1a. The exposure to the air coated an oxide shell on the Pb particles before transferring to the TEM. After the particle is melted in the TEM, the original crystalline Pb core turns to liquid abruptly. The change of the diffraction contrast results in the visualization of the oxide shell [15]. It may be not clear enough for POS since the amorphous support film contributes to a noisy background sometimes. The other is the cavity from the evaporation. It can be seen in the points marked by the arrows in Fig. 2d, where some material from the melted core is evaporated soon due to the low heat of evaporation of Pb. The abruptly enhanced evaporation is subject to the transition to liquid, which shows the melting point has passed then. Appearance of the cavities also eliminates the influence of superheating due to close oxide coating [16].

Figure 2 shows the evidence of melting retardation. Here, we trace the change of two particles, one of which is POC and the other is POS (Fig. 2b–c). Three tiny dots on the film demonstrate that the particles are well tracked. Figure 2a is the original image of the system at the temperature of 200 °C. All the particles were stable until the temperature reached 300 °C. A tiny cavity appeared inside

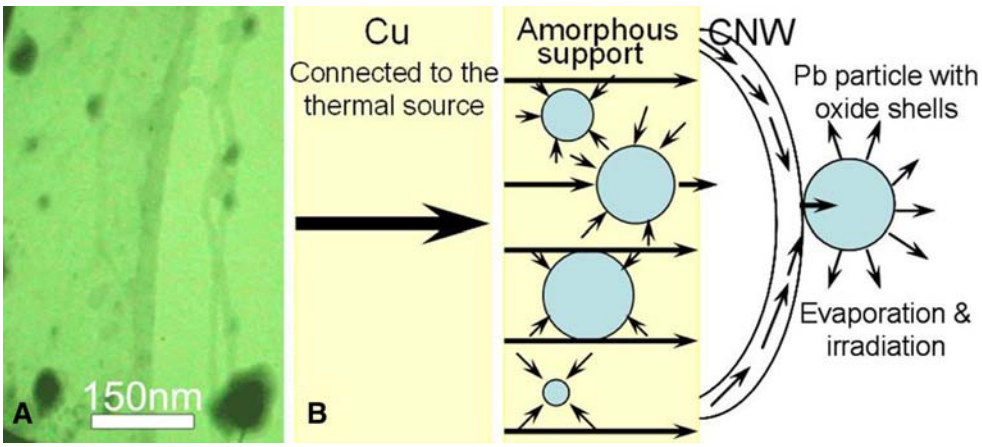

Fig. 1 The experimental configuration and schematic show of heat flow. **a** is the TEM image of the whole device, where we can see the nanowire is suspended on the hole of a porous carbon film. It was directly taken from the phosphorus screen by a digital video machine when the system was heated to 350 °C. **b** shows the schematic heat flow marked by the *arrows*

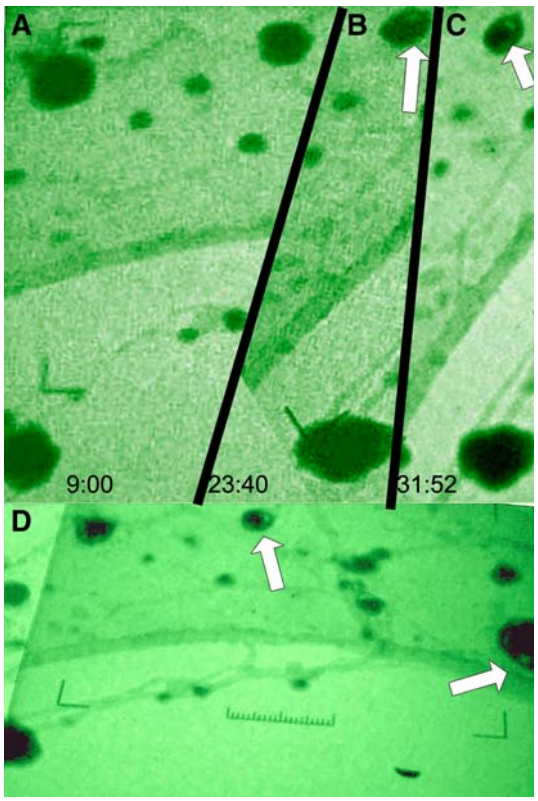

Fig. 2 The evidence for retardation of particle melting. **a**, **b** and **c** are the TEM images taken at the time of 9', 23'40" and 31'52", respectively. As recorded by the thermocouple, the corresponding heating temperatures are 200, 300 and 325 °C. The irregular edges of the insets are due to the cut of the frames from the DV. The sample kept shrinking when it was heated. The *arrows* point to the light vacancies due to the evaporation of the cores. (*d*) was taken at the heating temperature of 310 °C. It shares the same *scales bar* as (**a**)

the POS as shown in Fig. 2b at 300 °C and kept growing during further heating, demonstrating its melting. Some POS even collapsed. No obvious signature of melting occurred in POC after 7 min of heating at 300 °C. With increasing the heating temperature, the POC melted as shown by Fig. 2c, where a clear oxide shell can be seen. The earliest appearance of the oxide shell was at 310 °C (Fig. 2d). It was read from the thermocouple meter, and it was the temperature of the support film, when the POC was just beginning to melt. The melting of POS occurred before 300 °C. Assuming the equivalence of the melting points of all the Pb particles, the evidence with a TD of more than 10 K is present along the CNW. One may argue that the melting retardation is due to the size effect of Pb nanoparticles. But the size effect makes little influence on the melting points of the nanoparticles larger than 10 nm [19, 20], while the Pb particles in the experiment are larger than 50 nm. Furthermore, we can observe the evaporation of a very large POS (Fig. 2d). It occurs simultaneously with the evaporation of other POSs. It eliminates the influence of the size-dependent melting point and consolidates the presence of the earlier mentioned TD.

As stated earlier, the TD of up to 10 K between the two ends of less than 1 μm has been demonstrated. Such a TD is unexpectedly high since it turns out a thermal insulting performance of 10^4 K/mm. It could not be the result from the dominance of thermal transportation along CNW, as shown by the top calculation curve in Fig. 3a [19, 21].[1] If only the thermal transportation due to the TD contributes to the heat flow of the POC, the TD can cease to almost zero shortly. For example, if we increase the heating temperature from 573 to 623 K from one end of the CNW, the TD reduces to 0.1 K in ten milliseconds. The heavier mass of the POC contributes little to the TD. After considering the overall sources of thermal input and thermal dissipation of the POC, the irradiation is found to be an effective thermal dissipation route. Firstly, the convection through the air is excluded due to the high-vacuum environment. Secondly, thermal conduction through the CNW is the heat source. Final dissipation source of the irradiation can be described by the Stefan-Boltzmann Law $P = S\varepsilon\sigma \cdot T^4$, where S is the area of POC, ε of 0.43 is the emission coefficient of the grey body (oxided Pb) and σ is the constant. Although the irradiation effect is often omitted in the thermal measurement at a few hundred Celsius degrees [13], it is actually related to the surface area. In the experiment, a huge Pb particle is attached on the CNW, leading to a much larger surface than the original CNW and a larger irradiation thermal dissipation. It could be a reasonable explanation as shown by the calculation in Fig. 3b. The calculation considers the CNW thermal input, the irradiation dissipation and the temperature increase from heating. One can find the TD increases with increasing the size of POC. During heating from 673 to 723 K, the stable TD is still smaller than 0.5 K when the diameter is equal to that of CNW. It is consistent to the omittance in normal thermal measurement [13]. While POC becomes a ball with the radius of 65 nm, the TD of 4.5 K can be expected. The particle with the radius of 100 nm leads to a TD of nearly 10 K. The calculation validates the presence of the obvious TD in the experiment. It provides the TD of more than 1 K

[1] $\Delta T = \left(\frac{T_D \cdot \omega \cdot s}{l} - S\varepsilon\sigma T^4 - Q_0 e^{-Ev/KT}\right)/cm$, in which c, m and S are the specific heat, the mass and the surface area of the POC respectively. s, l and ω are the cross section, the length and the thermal conduction coefficient of the CNW. T is the temperature and Td is the TD between the two ends of the CNW. The first item is the thermal input from the CNW conduction; the second item is the irradiation of the grey body, $\varepsilon = 0.43$ is the emission coefficient of the oxided Pb; The third item describes the evaporation dissipation, where $Ev = 2.9$ eV stands for the heat of evaporation of lead. (from engieeringbox.com). The formula is employed for the calculation of Figs. 3 and 4. The time step of 1 ms is used. The thermal conductivity of 0.2 W/k m is used according to the previous measurement and the sp3 ratio (less than 10%) of the current CNW.

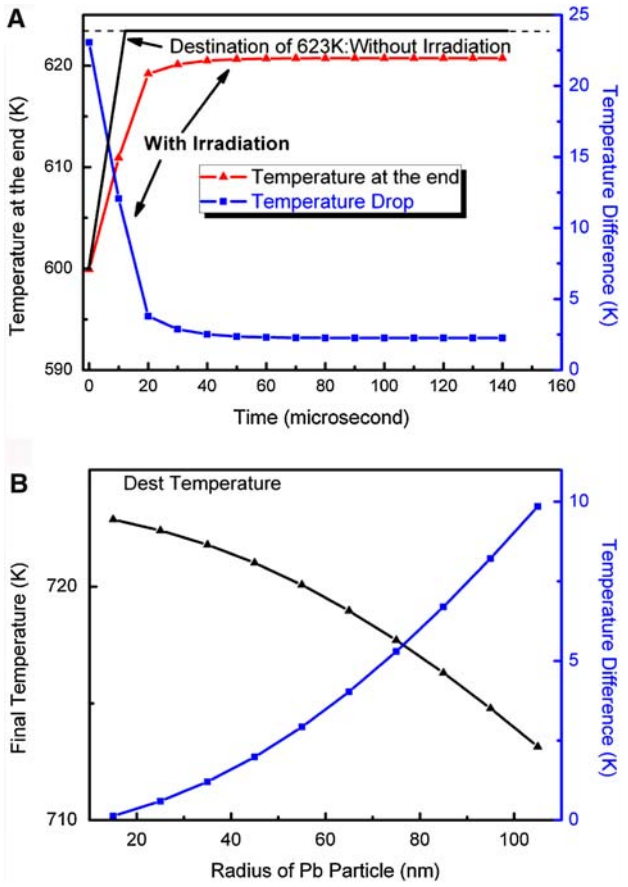

Fig. 3 The influence of the irradiation on the TDs. **a** assuming the heating temperature of 623 K at one end of the CNW and particle radius of 65 nm, we calculated the temperature at the other end. The calculation gives the result without considering the irradiation by the *smooth line* and shows the result considering the irradiation by the *red triangular-dot curve*. TD is the *box-dot curve*. **b** describes the influence of the radius of the Pb particle on its temperature and the TD along the nanowire. The decreasing *curve plots* the temperature of the Pb particle against its radius and the rising *curve plots* the TD. The *left axes* of both the *insets* are the Pb particle's temperature and the *right axes* are the TD. The heating temperature is assumed 723 K. (Color figure online)

at room temperature, which can be compared with the previous study [8, 10, 11].

Effective thermal dissipation in the cold end generates the obvious TD. Some other approaches of thermal dissipation are also considered. The absorption of the heat of melting makes much less contribution than the thermal input from TD driven thermal conduction. The fixed melting point of the POC during heat absorption increases its temperature abruptly, which ceases by the enhanced input immediately. The thermal evaporation is also considered. As shown in Fig. 4a–d, the evaporation of the Pb core increases with increasing the heating temperature. Here, we found that the evaporation is readily controlled when compared to POS. The evaporation of the POC becomes as obvious as that of POS after the heating temperature of 350 °C. Considering the heat dissipation from

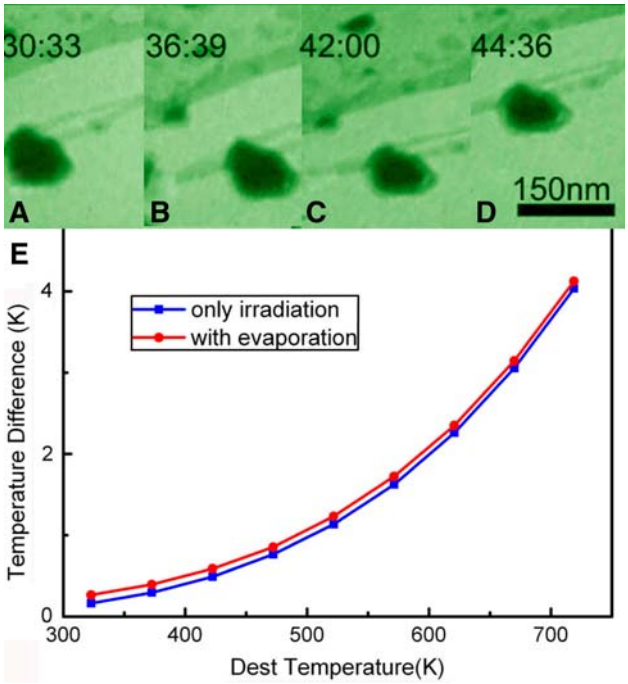

Fig. 4 The evidence of the retarded evaporation. **a**, **b**, **c** and **d** are the TEM images taken at the heating temperatures of 310, 350,400 and 450 °C, respectively. One can find the growth of the cavity inside the particle. The evaporation rate estimated from the images agrees to the estimation from the bulk value of heat of vaporization. Assuming the particle radius of 65 nm and the evaporation rate of $e^{-Ev/kT}$, the influence of the evaporation on the TD is assessed, resulting in the *round-dot curve* (irradiation + evaporation) and the *box curve* (only irradiation) in (**e**). The *x* axis of test temperature means the heating temperature

the evaporation, it gives the curves in Fig. 4e. From the curves, the little influence of the TD from the evaporation is concluded.

Conclusion

The obvious TD has been demonstrated along an amorphous CNW of less than 1μm decorated by the Pb nanoparticles. The irradiation effect enhanced by the larger surface of POC drives the obvious TD. The melting and the evaporation of the on CNW-Pb particle are retarded by the confined thermal transportation along the CNW. Such a phenomenon could give the hint of the future fabrication of thermoresistive materials.

Acknowledgments This work was financially supported by the National Natural Science Foundation of China (Grant No. 90606002, 10674056 and 10904065), the National Key Projects for Basic Research of China (Grant No. 2009CB930501, 2010CB923401). The authors acknowledge Mr. Jianming Hong (Nanjing University) for the technical assistance and Dr. Xuefeng Wang (Suzhou University) for thoughtful discussions.

References

1. G. Joshi, H. Lee, Y. Lan, X. Wang, G. Zhu, D. Wang, R.W. Gould, D.C. Cuff, M.Y. Tang, M.S. Dresselhaus, G. Chen, Z. Ren, Nano Lett. **8**(12), 4670 (2008)
2. B. Yoo, F. Xiao, K.N. Bozhilov, J. Herman, M.A. Ryan, N.V. Myung, Adv. Mater. **19**, 296 (2007)
3. A.S. Arico, P. Bruce, B. Scrosati, J.M. Tarascon, W. Van Schalkwijk, Nature Mater. **4**, 366 (2005)
4. J.G. Snyder, J.R. Lim, C.-K. Huang, J.P. Fleurial, Nature Mater. **2**, 528 (2003)
5. Y. Dubi, M. Di Ventra, Nano Lett. **9**(1), 97 (2009)
6. A. Boukai, K. Xu, J.R. Heath, Adv. Mater. **18**, 864 (2006)
7. E.A. Homann, J.E. Matthews, N. Nakpathomkun, A.I. Persson, H. Linke, Nano Lett. **9**(2), 779 (2009)
8. Y. Zhang, J. Christofferson, A. Shakouri, D. Li, A. Majumdar, Y. Wu, R. Fan, P. Yang, IEEE Trans. Nanotech. **5**(1), 67 (2006)
9. H.-L. Zhang, J.-F. Li, B.-P. Zhang, K.-F. Yao, W.-S. Liu, H. Wang, Phys. Rev. B **75**(1), 205407 (2007)
10. J. Hone, I. Ellwood, M. Muno, A. Mizel, M.L. Cohen, A. Zettl, A.G. Rinzler, A.E. Smalley, Phys. Rev. Lett. **80**(5), 1042 (1998)
11. M.E.T. Molares, N. Chtanko, T.W.C. Cornelius, D. Dobrev, I. Enculescu, R.H. Blick, R. Neumann, Nanotechnology **15**, S201 (2004)
12. T.W.C. Cornelius, F. Volklein, M.E. Toimil Molares, S. Karim, R. Neumann, presented at the proceedings of European conference on thermalelectrics (Cardiff, 2006; unpublished)
13. L. Shi, D. Li, C. Yu, W. Jang, D. Kim, Z. Yao, P. Kim, A. Majumdar, J. Heat Transfer **125**(5), 881 (2003)
14. E.A. Hoffmann, N. Nakpathomkun, A.I. Persson, H. Linke, H.A. Nilsson, L. Samuelson, Appl. Phys. Lett. **91**, 252114 (2007)
15. Z.W. Liu, Y. Bando, M. Mitome, J. Zhan, Phys. Rev. Lett. **93**, 095504 (2004)
16. F. Banhart, E. Hernandez, M. Terrone, Phys. Rev. Lett. **90**, 185502 (2003)
17. A. Stella, A. Migliori, P. Cheyssac, R. Kofman, Europhysics. Lett. **26**, 265 (1994)
18. F.Q. Song, M. Han, M.D. Liu, B. Chen, J.G. Wan, G.H. Wang, Phys. Rev. Lett. **94**, 093401 (2005)
19. P. Jensen, Rev. Mod. Phys. **71**(5), 1695 (1999)
20. G.M. Pastor, J. Dorantes-Davila, K.H. Bennemann, Chem. Phys. Lett. **148**, 459 (1988)
21. A.J. Bullen, K.E. O'Hara, D.G. Cahill, O. Monteiro, A. von Keudell, J. Appl. Phys. **88**, 6317 (2000)